

Dynamics and control strategies of infectious disease under different scenarios on hierarchical geographical networks

Xun Ma(马勋)[1,2,3], Ya-Peng Cui(崔亚鹏)[1,2,3], Xiao-Li Yan(闫小丽)[1,2,3], Shun-Jiang Ni(倪顺江)[1,2,3], Shi-Fei Shen(申世飞)[1,2,3]
Citation: Chin. Phys. B . 2019, 28(12): 128901 . **doi:** 10.1088/1674-1056/ab53ce
Journal homepage: http://cpb.iphy.ac.cn; http://iopscience.iop.org/cpb

What follows is a list of articles you may be interested in

Uncovering offline event similarity of online friends by constructing null models

Wenkuo Cui(崔文阔), Jing Xiao(肖婧), Ting Li(李婷), Xiaoke Xu(许小可)
Chin. Phys. B . 2019, 28(6): 068901 . **doi:** 10.1088/1674-1056/28/6/068901

Traffic dynamics considering packet loss in finite buffer networks

Jie Chen(陈杰), Jin-Yong Chen(陈金邕), Ming Li(李明), Mao-Bin Hu(胡茂彬)
Chin. Phys. B . 2019, 28(4): 048901 . **doi:** 10.1088/1674-1056/28/4/048901

Time-varying networks based on activation and deactivation mechanisms

Xue-Wen Wang(王学文), Yue-E Luo(罗月娥), Li-Jie Zhang(张丽杰), Xin-Jian Xu(许新建)
Chin. Phys. B . 2017, 26(10): 108902 . **doi:** 10.1088/1674-1056/26/10/108902

Link prediction in complex networks via modularity-based belief propagation

Darong Lai(赖大荣), Xin Shu(舒欣), Christine Nardini
Chin. Phys. B . 2017, 26(3): 038902 . **doi:** 10.1088/1674-1056/26/3/038902

Multiple-predators-based capture process on complex networks

Rajput Ramiz Sharafat, Cunlai Pu(濮存来), Jie Li(李杰), Rongbin Chen(陈荣斌), Zhongqi Xu(许忠奇)
Chin. Phys. B . 2017, 26(3): 038901 . **doi:** 10.1088/1674-1056/26/3/038901

Dynamics and control strategies of infectious disease under different scenarios on hierarchical geographical networks*

Xun Ma(马勋)[1,2,3], Ya-Peng Cui(崔亚鹏)[1,2,3], Xiao-Li Yan(闫小丽)[1,2,3], Shun-Jiang Ni(倪顺江)[1,2,3,†], and Shi-Fei Shen(申世飞)[1,2,3]

[1] *Institute of Public Safety Research, Tsinghua University, Beijing* 100084, *China*
[2] *Department of Engineering Physics, Tsinghua University, Beijing* 100084, *China*
[3] *Beijing Key Laboratory of City Integrated Emergency Response Science, Beijing* 100084, *China*

(Received 20 July 2019; revised manuscript received 26 September 2019; published online 29 November 2019)

Human settlements are embedded in traffic networks with hierarchical structures. In order to understand the spreading mechanism of infectious diseases and deploy control measures, the susceptible-infected-removed spreading process is studied with agents moving globally on the hierarchical geographic network, taking into account agents' preference for node layers and memory of initial nodes. We investigate the spreading behavior in the case of global infection under different scenarios, including different directions of human flow, different locations of infection source, and different moving behaviors of agents between layers. Based on the above-mentioned analysis, we propose screening strategies based on layer rank and moving distance, and compare their effects on delaying epidemic spreading. We find that in the case of global infection, infection spreads faster in high layers than in low layers, and early infection in high layers and moving to high layers both accelerate epidemic spreading. Travels of high-layer and low-layer residents have different effects on accelerating epidemic spreading, and moving between high and low layers increases the peak value of new infected cases more than moving in the same layer or between adjacent layers. Infection in intermediate nodes enhances the effects of moving of low-layer residents more than the moving of high-layer residents on accelerating epidemic spreading. For screening measures, improving the success rate is more effective on delaying epidemic spreading than expanding the screening range. With the same number of moves screened, screening moves into or out of high-layer nodes combined with screening moves between subnetworks has better results than only screening moves into or out of high-layer nodes, and screening long-distance moves has the worst results when the screening range is small, but it achieves the best results in reducing the peak value of new infected cases when the screening range is large enough. This study probes into the spreading process and control measures under different scenarios on the hierarchical geographical network, and is of great significance for epidemic control in the real world.

Keywords: disease spreading, hierarchical geographical networks, screening strategies

PACS: 89.75.Hc **DOI:** 10.1088/1674-1056/ab53ce

1. Introduction

Epidemic spreading has been a global issue owing to fast development of transportation systems. Establishing more realistic epidemic spreading models is of great significance for understanding the mechanism of the spreading process and taking appropriate control measures. Traditional compartment models such as the susceptible-infected-removed (SIR) and susceptible-infected-susceptible (SIS) models[1] assume random and homogeneous mixing of population, and each member in a compartment is treated similarly and indistinguishably from the others in the same compartment, ignoring the contact structure of individuals. Network models[2–5] can grasp contact structures among people and have been a major approach to study epidemic spreading via human contacts, e.g., severe acute respiratory syndrome and influenza. However, contact structure varies when human moves between settlements, and network models neglect the diffusion of human. Therefore, metapopulation network models[6–8] are proposed where nodes represent subpopulations such as countries, cities and districts within a city, or even shopping malls, schools and homes, and links between the nodes represent traffic routes between subpopulations. The metapopulation models assume random and homogeneous mixing within subpopulations and human can diffuse along the links. Metapopulation network models are widely used in epidemic spreading with human moving, especially large-scale spatial spreading of epidemic through civil aviation and railway networks.[9–13]

In recent years, structure of metapopulation networks has been a hot spot due to its significant influence on human moving and epidemic spreading. Researchers have shown that degree heterogeneity of metapopulation network could sustain the reaction activity in the limit of vanishing density of particles, suppressing the critical point in density-driven phase transitions,[14] and strong heterogeneity would lead to high degree of predictability for globally spreading epidemics.[15] Modularity and assortativity, i.e., rich-club property, also have

*Project supported by the National Key R&D Program of China (Grant No. 2018YFF0301005), the National Natural Science Foundation of China (Grant Nos. 71673161 and 71790613), and the Collaborative Innovation Center of Public Safety, China.

†Corresponding author. E-mail: sjni@tsinghua.edu.cn

© 2019 Chinese Physical Society and IOP Publishing Ltd

deep impact on the spreading velocity and outbreak size.[16,17] In addition, influence of more complicated structures is studied. In multiscale mobility networks, compared with long-range airline traffics, short-scale commuting flows were found to contribute little to global spreading of epidemics.[18] By analyzing the data regarding epidemic of measles and pertussis in Iceland during 1888–1990, Watts *et al.* found that the distribution of outbreak size is not bimodal as it is generally believed, but rather flat, and the new cases are resurgent throughout an outbreak of the epidemic. Different from previous human moving models that were restricted to mixing on two scales, which were called "local" and "global", Watts *et al.* considered the traffic network as multi-layered and human moving as multi-scaled, and established a hierarchical metapopulation model which could well explain the extreme size variation and temporal heterogeneity.[19] To mimic multiscale mobility behaviors and the organization of traffic systems embedded in realistic geography, Han *et al.*[20] proposed a hierarchical geographic network model, upon which a random walker generated a power-law-like travel displacement distribution with tunable exponents, in accordance with empirical observations reported by Brockmann *et al.*[21] Also, Zhao *et al.*[22] found a hierarchical structure contributed to the resurgent and multiscale behavior of epidemics, implying high unpredictability of epidemic spreading. Moreover, Han *et al.*[23] studied epidemic spreading on hierarchical geographical networks with randomly walking agents, clarifying the relation between epidemic peak timing and pertinent demographic factors and providing a quantitative discussion of the efficiency of a border screening procedure focused on delaying epidemic outbreaks by reducing long-range travels.

Apart from the metapopulation network structure, human behavior is also an important factor to consider in epidemic spreading. More and more studies have shown that the timing of many human activities, ranging from communication to entertainment and work patterns, follow non-Poisson statistics, characterized by bursts of rapidly occurring events separated by long time of inactivity, rather than Poisson distribution assuming that human actions are randomly distributed in time.[24–26] Non-Poisson nature of the contact dynamics results in slowing down of the spreading and prevalence decay time significantly larger than that predicted by the standard Poisson process based models,[27,28] which mainly stems from weight-topology correlation and the burst activity pattern of individuals.[29] Human moving trajectories also exhibit non-Poisson characteristics. Brockman *et al.*[21] analyzed the disposal of bank notes in the United States and extracted the scaling laws of human travel, i.e., the human travel distance r and the rest time t_{w} between displacements obey the heavy-tailed distribution $p(r) \sim r^{-(1+b)}$ and $p(t_{\mathrm{w}}) \sim t_{\mathrm{w}}^{-(1+a)}$, respectively, where they predicted $a = b = 0.6$. Further, similar results were found by studying the trajectories of mobile phone users whose position was tracked, with individuals' significant probability to return to a few highly frequented locations.[30] Based on the findings, Ni and Weng[31] studied the impact of travel pattern on epidemic dynamics in heterogeneous spatial networks and clarified the significant dependence of occurrence probability of global outbreaks on travel distance, waiting time and memory effects of human travel. Wang *et al.*[32] found that due to the human mobility pattern, Bluetooth viruses spread slowly, offering ample time to deploy countermeasures. Apart from the non-Poisson property, influence of other moving behaviors was studied. Compared with random walk, recurrent mobility patterns rendered saturation of the spreading velocity with an increasing travelling rate,[33–35] while dynamical condensation[36,37] and objective travelling[38] through shortest path from origin to destination facilitated epidemic spreading. By analyzing human mobility data captured by mobile-phone traces, Song proposed an explore and preferential return model, which stressed the preference for frequently visited locations and explained the mechanism of number of distinct locations visited, visitation frequency and ultraslow diffusion in human moving process. Barbosa further found that human not only tended to move to frequently visited locations, but also had preference for recently visited locations. Therefore, the random walk model cannot accurately describe human moving process.

In view of the above analysis, this paper establishes an epidemic spreading model with agents moving globally with layer preference and memory of initial nodes on a hierarchical geographical network. We first investigate on human moving and epidemic spreading under different scenarios, including different directions of human flow, locations of infection source, and moving behaviors between agents in each layer. Based on the analysis, we propose mitigation strategies respectively focusing on high-layer nodes and long-distance moves, and compare their effects on delaying epidemic spreading.

2. Model

The epidemic spreading model in this paper consists of three sub-models: network model, human mobility model, and local infection model.

2.1. Network model

We use the form of hierarchical geographical network model reported in Ref. [20] to describe the transportation system in the real world. There are H layers with N_1 nodes in the first layer and node number expansion rate q between layers h and $h-1$, thus the number of nodes in layer h is

$$N_h = N_1 \times q^{h-1}, \tag{1}$$

and the total number of nodes is

$$N = \frac{N_1(q^H - 1)}{q - 1}. \tag{2}$$

Each node is randomly distributed in an $S \times S$ continuous square with a pair of values of x and y within the interval $[0, S)$ to represent its coordinates. It should be noted that the Euclidean distance between each pair of nodes is measured under the periodic conditions, thus the maximum Euclidean distance between two nodes is $S\sqrt{2}/2$. Further, to study epidemic spreading on different scales, the whole network is divided into N_1 subnetworks by the N_1 first-layer nodes and the lower-layer nodes under them, thus moving and infection within or among the subnetworks are considered to be local or global, respectively.

2.2. Human mobility model

The total number of agents in the system is $M = A \times N$, where A is the average number of agents in a node. Each agent i is assigned to an initial node n, corresponding to its permanent residence in the real world, and agent i is called a resident of its initial node n. Probability of i assigned to n is proportional to ω^{h_n}, where h_n is the layer of n, and $0 < \omega < 1$ is to adjust the difference of average number of residents in a node between each layer. Agents are all located in their initial nodes before the moving process begins.

We consider that agents move globally with preference for layers and memory of initial nodes. A highly developed traffic system enables human to arrive in any corner of the world in one day, thus in the model, agents can visit any node in the network in a time step, which is different from most metapopulation network models where agents can only visit neighbor nodes of their current nodes in a time step. Human moving process is modeled as follows.

(i) **Travel** For each agent i located in its initial node n, at each time step, i leaves n with probability p_{travel} and enters node m along the shortest path with the probability

$$p(n \to m) \sim \frac{h_m^{\mu}}{q^{h_m - 1} N_1} \times \frac{d_{mn}^{-(1+\beta)}}{N(d_{mn})}, \tag{3}$$

then it goes to step (ii); otherwise, i stays in node n and goes to step (i) again at the next time step. Here h_m is the layer of m, $q^{h_m - 1} N_1$ is the number of nodes in layer h_m, d_{mn} is the distance between n and m, which is the sum of Euclidean distances between adjacent pairs of nodes along the shortest path from n to m. To count the number of nodes at different distances from a node, we divide the distance between nodes into several intervals, each of which has a length of $S/100$, and $N(d_{mn})$ is the number of nodes whose distance from n is within the distance interval of d_{mn}. The first item on the right side of Eq. (3) expresses the preference for layers with an adjustable parameter μ, and $\mu > 0$ means that agents tend to enter low-layer nodes when they move, otherwise agents tend to move to high-layer nodes. Therefore, the value of μ determines the direction of the human flow. The second item on the right side of Eq. (3) expresses the preference for distance when agents move with an adjustable parameter β.

(ii) **Wait** When i arrives in node m, it will be assigned a waiting time t_{w} that is drawn from the heavy-tailed distribution $p(t_{\text{w}}) \sim t_{\text{w}}^{-(1+\alpha)}$ $(1 \leqslant t_{\text{w}} \leqslant T_{\max})$, where α is an adjustable parameter governing the distribution of t_{w} and $T_{\max}$ is the maximum waiting time in a non-initial node. Here i stays in m for t_{w} time steps then goes to step (iii).

(iii) **Return or drift** After waiting for t_{w} time steps in node m, i will return back to its initial node n along the shortest path with probability p_{return}, then starts again from step (i) at the next time step; otherwise, it will drift to another non-initial node j that is chosen according to Eq. (3), followed by step (ii).

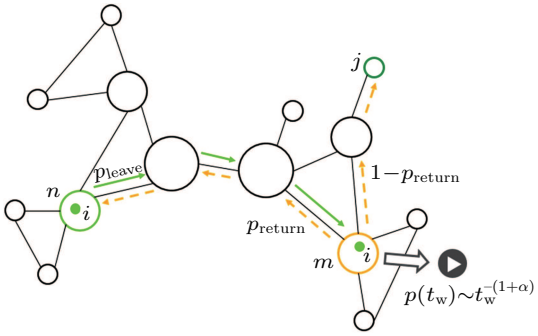


Fig. 1. Human moving process in a hierarchical geographical network with $H = 3$ and $q = 2$. Larger nodes represent higher-layer settlements.

2.3. Local infection model

Local infection process is described by the SIR model. At each time step, each agent contacts with k other agents in the same node. In addition, each agent that moves at the time step additionally contacts with k other agents in each intermediate node it passed between the origin node and the destination node during the move. When a susceptible agent contacts with an infected agent, the susceptible one gets infected with probability p_{SI} if the contact occurs neither in the intermediate nodes of the infected agent nor in the intermediate nodes of the susceptible agent, or with probability $r \times p_{\text{SI}}$ otherwise. At the same time, infected agents are removed with probability p_{IR} at each time step.

At the first time step, agents are all susceptible and located in their initial nodes. In order to make the population distribution stable in each layer, we let agents move under the model rules for 1000 time steps before the infection is introduced. We set the initial infection in layer h_{init} by randomly choosing an agent in h_{init} as the initial infector, i.e., infection source. We fix the model parameters as default parameter settings in all the following discussions, unless a given parameter

value is differently specified: the network parameters $S = 100$, $H = 4$, $N_1 = 6$, $q = 6$, thus $N = 1554$; the human moving parameters $A = 100$, $M = 155400$, $\omega = 0.5$, $p_{\text{travel}} = 0.005$, $p_{\text{return}} = 0.8$, $\mu = 0$, $\beta = \alpha = 0.6$ and $T_{\max} = 365$; and the infection parameters $k = 5$, $p_{\text{SI}} = 0.06$, $p_{\text{IR}} = 0.1$, $r = 0$ and $h_{\text{init}} = 1$.

3. Simulation results

3.1. Human moving and epidemic spreading under different scenarios

According to Ref. [21], the Euclidean distance of human moving obeys power-law distribution $p(r) \sim r^{-(1+b)}$, which can also be generated in our model. Figure 2(a) shows the power-law exponent b decreases from 1.55 to 0.42, as μ decreases from 2.0 to -2.0, indicating that moving to high layers increases the frequency of long-range moves. The proportion of global moves between different subnetworks decreases as μ increases, as shown in Fig. 2(b), because of the shorter distance between high-layer nodes and other subnetworks. In addition, we compare the number of intermediate nodes in a move of the residents of each layer. Figure 2(c) shows that residents of low layers pass more intermediate nodes in a move than residents of high layers. In addition, moving to high layers further reduces the number of intermediate nodes for high-layer residents, while it increases the number of intermediate nodes for low-layer residents.

Spreading velocity and propagation scale are two important concerns in epidemic spreading dynamics. In the SIR model, the spreading velocity is often measured by the peak timing of new infected cases, and the propagation scale is measured by the proportion of the removed agents at the end of the infection, i.e., at the time when there are no infected agents left. However, propagation scale is not appropriate to measure the spreading risk, due to the different spreading behaviors, including surging or ultra-slow increase of the infected agents, and rapid extinction or ultra-slow decrease of them. For example, slowly increasing the number of infected agents with long time scale leads to large propagation scale, but the risk is low due to the sufficient time to deploy mitigation measures. Therefore, more attention should be paid to the spreading velocity in the case-growing phase of the spreading process. The peak timing of new infected cases is also not enough to measure the spreading velocity, because it only expresses the time it takes for an infection to reach its maximum value of new infected cases, i.e., the peak value, and the peak value is also an important index of the spreading velocity. In this study we focus on large-scale spreading of epidemics, i.e., global spreading, in which infected nodes exist in every subnetwork. In this case, the peak value and peak timing of new cases, respectively represented as $C(\tau)$ and τ, are used to measure the velocity of the spreading, with larger $C(\tau)$ and smaller τ corresponding to larger spreading velocity.

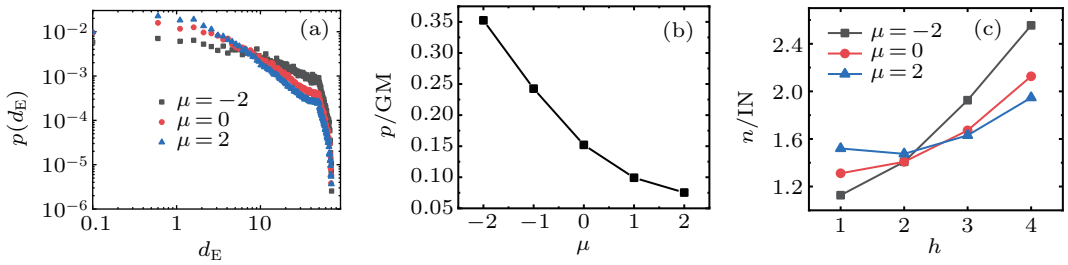


Fig. 2. Impact of preference for layers on human moving behavior. (a) The move-length distribution of agents under different μ, where the move length is measured by the Euclidean distance. (b) The proportion of global moves as a function of μ. (c) The number of intermediate nodes in a move of residents of each layer under different μ. All the results are averaged by 100 runs, each of which lasts for 10^3 time steps.

We first investigate the influence of h_{init} and μ on the spreading velocity in each layer. Figures 3(a) and 3(b) display $C(\tau)$ and τ of each layer respectively in the case of different μ and h_{init}. Infection always spreads faster in high layers than in low layers regardless of the preference for layers and location of infection source, while moving to low layers and early infection in low layers reduce the difference of spreading velocity between high and low layers. This is because of the aggregation of agents in the relatively small number of high-layer nodes. Then we study the influence of h_{init} and μ on the overall spreading velocity. Figure 3(c) shows that the infection spreads faster when h_{init} is smaller, and smaller μ further accelerates epidemic spreading, indicating that early infection in the high-layer nodes and moving to the high-layer nodes both accelerate epidemic spreading. A node is infected when there are infected residents in it. Therefore, a node gets infected by two means: resident-induced infection and visitor-induced infection. Resident-induced infection is caused by the return of infected residents that get infected in other non-initial nodes, and visitor-induced infection is caused by residents of the node that get infected by infected visitors entering the node. Due to the faster infection in high-layer nodes, moving to the high-layer nodes increases the proportion of visitor-induced infection of high-layer nodes, while it reduces the proportion of visitor-induced infection of low-layer nodes, as shown in Fig. 3(d). This result also indicates that larger proportion of nodes in high layers get infected by visitor-induced infection than in low layers, and resident-induced infection is

the main form of node infection. Here h_{init} has little influence on the proportion of visitor-induced infection of each layer, as shown in Fig. 3(e). In the real world, moving behavior differences exist among residents of different layers due to the position in the traffic system and social relations. In this paper we mainly discuss two aspects of layer-related moving behavior differences that may have influence on epidemic spreading, i.e., travel frequency and preference for layers.

To represent the differences of travel frequency between residents of each layer, we first set the average travel probability of all the agents as p_{travel}, thus the average number of agents travelling from their initial nodes at each time step is $M_{\text{init}}(t) \times p_{\text{travel}}$, where $M_{\text{init}}(t)$ is the total number of agents that are in their initial nodes at time t. Next, we consider that the number of travelling agents of layer h is proportional to h^{λ} at each time step, where λ governs the degree of the difference in the number of agents travelling from each layer. Thus the number of agents travelling from layer h is

$$M^{h}_{\text{travel}}(t) = M_{\text{init}}(t) \times p_{\text{travel}} \times \frac{h^{\lambda}}{\sum_{h=1}^{H} h^{\lambda}}, \tag{4}$$

and the travel probability of agents of layer h is

$$p^{h}_{\text{travel}}(t) = \frac{M^{h}_{\text{travel}}(t)}{M^{h}_{\text{init}}(t)}. \tag{5}$$

For $\lambda = 0$, the number of travelling agents of each layer is equal, and larger λ means that there are more agents travel from low layers than from high layers. To ensure that residents in high layers do not run out, leading to insufficient population in high layers to continue the moving process, λ can not be too small.

Figure 4 exhibits $C(\tau)$ and τ versus λ. Figures 4(a) and 4(b) shows the case of $h_{\text{init}} = 1$ and $h_{\text{init}} = 4$, respectively, with no infection in the intermediate nodes considered, i.e., $r = 0$. Curves of $C(\tau)$ have different trends under different μ. $C(\tau)$ increases monotonically as λ increases from 0.0 to 4.0 in the case of $\mu = -2$, while $C(\tau_0)$ increases first and then decreases in the case of $\mu = 2$. This can be explained as follows. As residents in low layers are more dispersed, travel of low-layer residents is conducive to making residents of more nodes contact with each other. According to Figs. 3(a) and 3(b), agents in high layers get infected earlier. When μ is small, larger λ causes susceptible residents of more nodes to move up and contact with infected agents in high layers, thus increases resident-induced infection and $C(\tau_0)$ increases with λ. However, when μ is large, moving of low-layer residents no longer causes more resident-induced infection, due to more moves between low-layer nodes and contact between susceptible agents, which contribute little to the infection. At the same time, visitor-induced infection decreases as λ increases due to fewer infected agents travelling from high layers. Therefore, $C(\tau)$ first increases and soon decreases with λ in the case of $\mu = 2$. Here τ increases monotonically as λ increases. According to Fig. 3(c), moving to the high-layer nodes accelerates the spreading process. When λ is small, there are relatively more agents travelling from high layers, leading to easier exchange of agents between subnetworks due to the shorter distance between high-layer nodes and other subnetworks, which accelerates the spreading process and reduces τ.

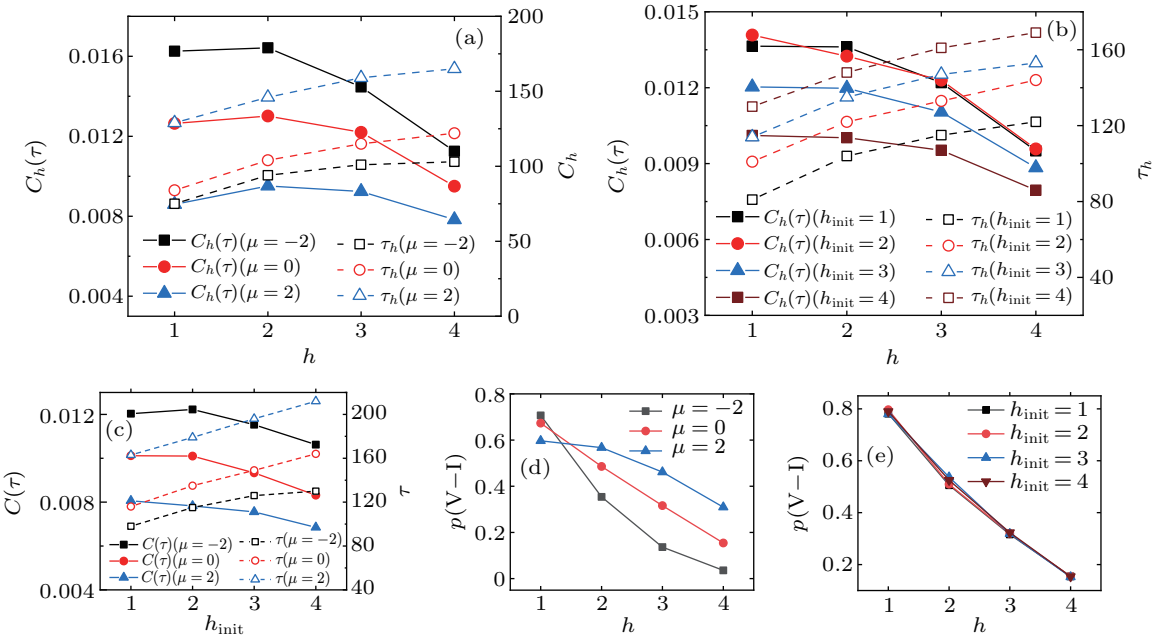


Fig. 3. Epidemic spreading under different preference for layers and location of infection source. (a) $C(\tau)$ and τ of agents in each layer under different μ. (b) $C(\tau)$ and τ of agents in each layer under different h_{init}. (c) Overall $C(\tau)$ and τ versus h_{init} under different μ. (d) Proportion of visitor-induced infection of nodes in each layer under different μ. (e) Proportion of visitor-induced infection of nodes in each layer under different h_{init}. Each point is generated from 500 simulations of global infection.

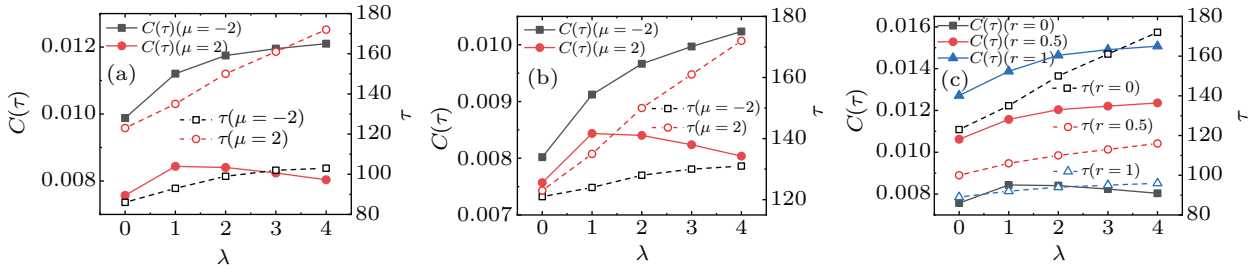


Fig. 4. Peak value $C(\tau)$ and peak timing τ versus λ: (a) $h_{\text{init}}=1$, $r=0$, (b) $h_{\text{init}}=4$, $r=0$, (c) $h_{\text{init}}=1$, $\mu=2$. The solid points represent $C(\tau)$ and hollow points represent τ. Each point is generated from 500 simulations of global infection.

Figure 4(c) shows the case that the infection in intermediate nodes is considered under $h_{\text{init}}=1$ and $\mu=2$. Different from the case of $r=0$, $C(\tau)$ increases monotonically with λ under $r=0.5$ and $r=1$. Larger r leads to larger difference in $C(\tau)$ and smaller difference in τ among cases of different λ. This is because low-layer residents go through more intermediate nodes than high-layer residents in a move, and when $r\neq 0$, larger λ makes low-layer residents participate in the infection of more high-layer intermediate nodes, take the infection to other susceptible high-layer nodes, and bring the infection to their initial nodes, thus increases $C(\tau)$ and reduces τ.

To study the influence of the difference of preference for layers between residents of each layer on epidemic spreading, we first set $\lambda=0$ to ensure that the number of agents moving from each layer is the same at each time step. We consider that residents of layer h has the same layer preference coefficient μ_h, and the layer preference coefficients of all layers are considered as an arithmetic progression, with the average value $\overline{\mu}$ and tolerance $\Delta\mu$. Thus the layer preference coefficient of residents of layer h is

$$\mu_h=\left(h-\frac{H+1}{2}\right)\times\Delta\mu+\overline{\mu}, \tag{6}$$

where $\overline{\mu}$ is set as 0, and $\Delta\mu>0$ means that residents of high layers are more inclined to moving to high-layer nodes and residents of low layers are more inclined to moving to low-layer nodes, while $\Delta\mu<0$ means the cross-layer moving pattern.

Figures 5(a) and 5(b) shows the cases of $h_{\text{init}}=1$ and $h_{\text{init}}=4$, respectively, with $r=0$. As can be seen from the figures, $C(\tau)$ decreases monotonically as $\Delta\mu$ increases. According to Figs. 3(a) and 3(b), infection spreads faster in high-layer nodes than in low-layer nodes. Cross-layer moving pattern enhances both visitor-induced infection by high-layer infected agents moving to low-layer susceptible nodes, and resident-induced infection by low-layer susceptible agents moving to high-layer infected nodes, thus increases $C(\tau)$. When $r=0$, τ first decreases then increases as $\Delta\mu$ increases under $h_{\text{init}}=1$, while τ increases monotonically under $h_{\text{init}}=4$. This phenomenon can be explained as follows. Larger $\Delta\mu$ makes moves between high-layer nodes more frequent, and when the infection source is in the high layers, the infection can quickly spread to all the high-layer nodes, thus accelerates the spreading process and reduces τ. However, larger $\Delta\mu$ also makes residents of low-layer nodes, which accounts for most part of the total population, move to low-layer nodes, slowing down epidemic spreading. Therefore, when $\Delta\mu$ is too large, τ increases. On the other hand, when the infection source is in low-layer nodes, smaller $\Delta\mu$ instead facilitates the quick infection of high-layer nodes due to the cross-layer moving pattern. It also makes low-layer residents move to high-layer nodes, which further accelerates the spreading process. Thus τ increases monotonically as $\Delta\mu$ increases.

Figure 5(c) shows the case that infection in intermediate nodes is considered for $h_{\text{init}}=1$. As r increases, the curve of τ gradually loses the decrease phase and increases monotonically. This is because larger r enhances the effects of cross-layer moving on the quick infection of high-layer nodes, by low-layer residents participating in the infection of more intermediate high-layer nodes when $\Delta\mu$ is small.

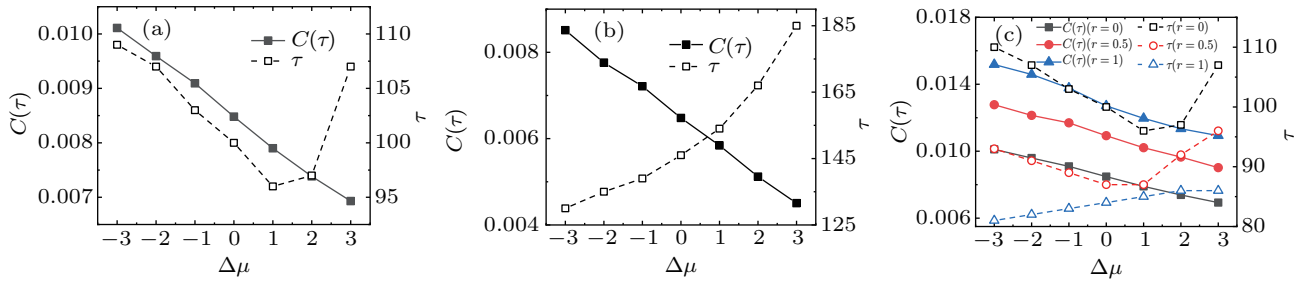


Fig. 5. Peak value $C(\tau)$ and peak timing τ versus $\Delta\mu$: (a) $h_{\text{init}}=1$, $r=0$, (b) $h_{\text{init}}=4$, $r=0$, (c) $h_{\text{init}}=1$. The solid points represent $C(\tau)$ and hollow points represent τ. Each point is generated from 500 simulations of global infection.

3.2. Screening strategies based on layer rank and moving distance

Border screening is a common strategy to prevent epidemics from spreading to other discrete settlements.[39,40] However, effectiveness of border screening is still controversial. For example, confronted with the bursts of severe acute respiratory syndrome (SARS), Chinese government implemented entry screening policy which turned out to be very effective in preventing SARS from spreading to more cities. However, some research on travel restriction stated that travel restriction is highly ineffective in containing epidemics.[10] In this paper, we propose two kinds of screening strategies respectively aiming at moves into or out of high-layer nodes, and moves of long distance.

As we know from the analysis above, moving to high-layer nodes is more conducive to reducing τ, and moving between high-layer and low-layer nodes is more conducive to increasing $C(\tau)$. Thus, strategy I is to weaken the spreading by shutting down high-layer nodes, i.e., preventing agents from moving into or out of high-layer nodes. On the other hand, global moves increase the contact range of agents and reduce the proportion of repeated contact between agents from different nodes, thus facilitates the spreading. Hence, to achieve better effects, preventing moves into or out of high-layer nodes should be together with preventing global moves, which is strategy Ⅱ.

In order to ensure the feasibility, for strategy I we choose nodes in the top two layers to implement move screening in sequence from 1^{st}-layer nodes to 2^{nd}-layer nodes, and nodes are chosen randomly in the same layer. As $N_1 = 6$ and $q = 6$, the maximum number of target nodes is $N_1 + N_2 = 42$ and $N_s = 6$ represents move screening for 1^{st}-layer nodes. For strategy Ⅱ, moves between subnetworks are also screened besides move screening for high-layer nodes. In addition, the probability that a chosen move is successfully screened is set as $p_s = 0.8$, which serves as the measure of success rate of the screening strategy. If a move is successfully screened when the agent is returning, then the return probability of the agent is 1 before the agent arrives in his initial node, representing that the trip out of the initial node is finished. Once the agent arrives in the initial node, his return probability is 0.8 again.

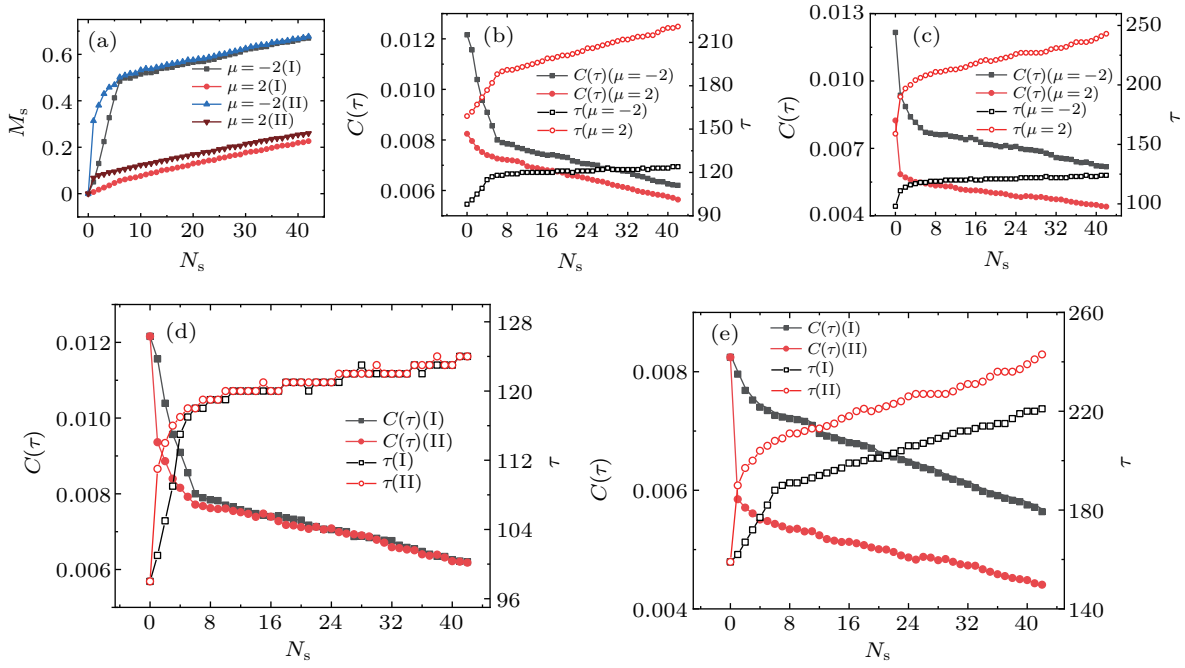


Fig. 6. Effects of strategy I and strategy Ⅱ on delaying epidemic spreading under different μ. (a) M_s versus N_s for strategy I and strategy Ⅱ under $\mu = -2$ and $\mu = 2$. (b) $C(\tau)$ and τ versus N_s for strategy I under $\mu = -2$ and $\mu = 2$. (c) $C(\tau)$ and τ versus N_s for strategy Ⅱ under $\mu = -2$ and $\mu = 2$. (d) $C(\tau)$ and τ versus N_s for strategy I and strategy Ⅱ under $\mu = -2$. (e) $C(\tau)$ and τ versus N_s for strategy I and strategy Ⅱ under $\mu = 2$. Each point is generated from 500 simulations of global infection.

Figure 6 exhibits the results of strategy I and strategy Ⅱ. Figure 6(a) shows the average proportion of moves screened out of all the moves in a time step before τ, which is represented as M_s, versus the number of target high-layer nodes N_s for strategy I and strategy Ⅱ under $\mu = -2$ and $\mu = 2$. These two strategies screen more moves when μ is smaller. M_s increases monotonically as N_s increases, and the curves have larger slope when $N_s \leqslant N_1 = 6$, especially under $\mu = -2$. In addition, strategy Ⅱ screens more moves than strategy I. The difference in M_s between the two strategies becomes smaller as N_s increases, and their difference is larger under $\mu = 2$ than under $\mu = -2$, indicating that screening for high-layer nodes can effectively screen out global moves when agents tend to move to high-layer nodes, but it is not effective when agents

move to low layers. Figures 6(b) and 6(c) show $C(\tau)$ and τ versus N_s under different μ respectively for strategy I and strategy II. The curves of $C(\tau)$ and τ for strategy I have similar trends with them for strategy II. $C(\tau)$ decreases monotonically as N_s increases, especially sharply when $N_s \leqslant N_1 = 6$, which is opposite to the trend of M_s versus N_s, while the curves of τ have similar trends with M_s versus N_s. Figures 6(d)–6(e) show the comparison of the effects between strategy I and strategy II respectively under $\mu = -2$ and $\mu = 2$. Strategy II has better effects in delaying epidemic spreading than Strategy I with the same value of N_s, and the difference of their effects increases under larger μ due to the enlargement of the difference of M_s according to Fig. 6(a).

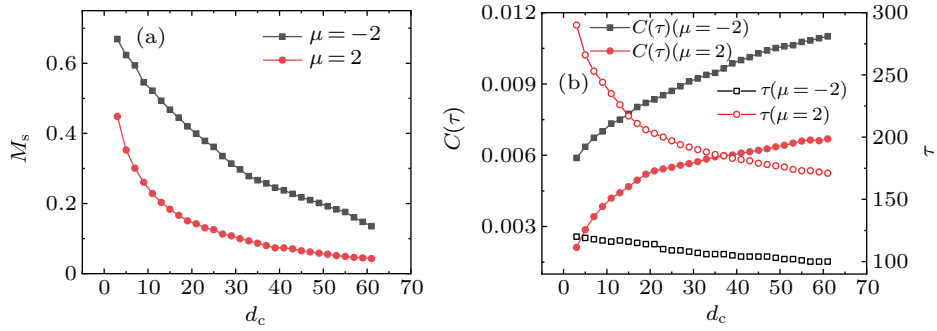


Fig. 7. Effects of strategy III on delaying epidemic spreading under different μ. (a) M_s versus d_c under $\mu = -2$ and $\mu = 2$. (b) $C(\tau)$ and τ versus d_c under $\mu = -2$ and $\mu = 2$. Each point is generated from 500 simulations of global infection.

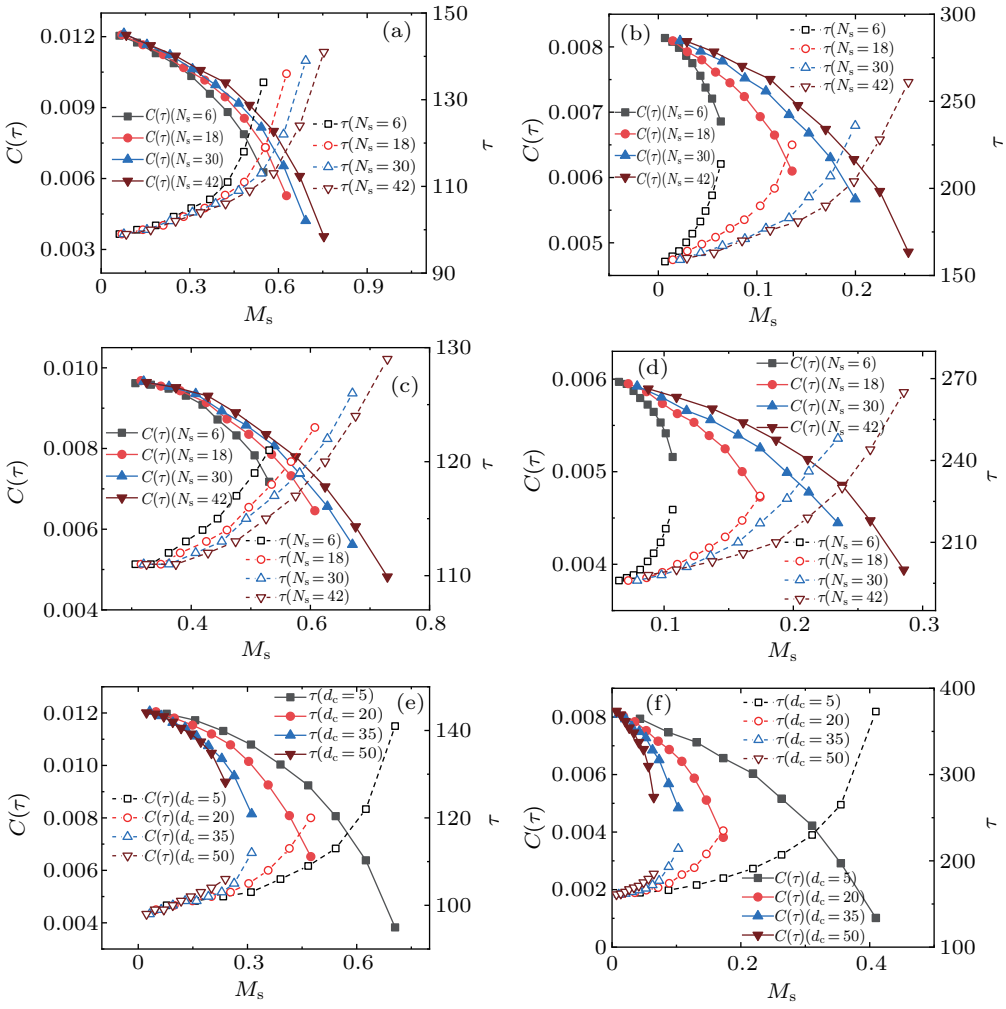


Fig. 8. $C(\tau)$ and τ of the three strategies versus M_s with different screening range and p_s from 0.1 to 0.9 under different μ. (a) Strategy I with $N_s = 6, 18, 30, 42$ under $\mu = -2$. (b) Strategy I with $N_s = 6, 18, 30, 42$ under $\mu = 2$. (c) Strategy II with $N_s = 6, 18, 30, 42$ under $\mu = -2$. (d) Strategy II with $N_s = 6, 18, 30, 42$ under $\mu = 2$. (e) Strategy III with $d_c = 5, 20, 35, 50$ under $\mu = -2$. (f) Strategy III with $d_c = 5, 20, 35, 50$ under $\mu = 2$. The solid points represent $C(\tau)$ and hollow points represent τ. Each point is generated from 500 simulations of global infection.

At the same time, we investigate on the screening strategy focusing on moves of long distance, which is strategy Ⅲ. Here we set the distance threshold d_c, and moves with distance that is larger than d_c at the time step will be screened with p_s. Figure 7(a) exhibits M_s as a function of d_c under $\mu = -2$ and $\mu = 2$.M_s decreases monotonically, and the curves of M_s become flatter as d_c increases. M_s under $\mu = 2$ decreases faster when d_c is small, while M_s under $\mu = -2$ decreases faster when d_c is large. The shape of the curves of M_s versus d_c depends on the distribution of the moving distance under different μ. Figure 7(b) exhibits $C(\tau)$ and τ versus d_c under different μ. Similarly, as d_c increases, the curves of $C(\tau)$ and τ become flatter. It is noticeable that strategy Ⅲ achieves better results in delaying epidemic spreading when μ is large, as τ under $\mu = 2$ increases much faster than τ under $\mu = -2$ as d_c decreases.

In the real world, M_s is an important factor to consider, and our goal is to minimize the value of M_s, at the same time meet the effects of delaying epidemic spreading. Expanding the screening range, i.e., increasing the number of target high-layer nodes for strategy I and strategy Ⅱ, or reducing the value of d_c for strategy Ⅲ, and increasing the success rate p_s, both can enhance the effects of delaying spreading, at the same time increase M_s. Thus, we discuss which method can achieve better results with the same M_s. Figure 8 shows the results of the three screening strategies with M_s in the case of different screening range and μ, and the value of M_s corresponds to different p_s in each case. Under the same value of M_s, smaller N_s with larger p_s has better effects than larger N_s with smaller p_s. Similarly, larger d_c with larger p_s has better effects than smaller d_c with smaller p_s for strategy Ⅲ. Their difference is larger under $\mu = 2$ than under $\mu = -2$. This indicates that increasing the success rate of screening strategies for higher-layer nodes and longer-distance moves is more effective in delaying epidemic spreading than expanding screening range.

According to Fig. 2, agents moving to high-layer nodes increases the frequency of global moves and long-distance moves. Therefore, strategy I, strategy Ⅱ and strategy Ⅲ have similar effects in delaying epidemic spreading. However, they still have their own characteristics. Figures 9(a)–9(f) exhibit the comparison of the results of the three strategies with M_s in the case of different p_s and μ, and the value of M_s corresponds to different screening range in each case.

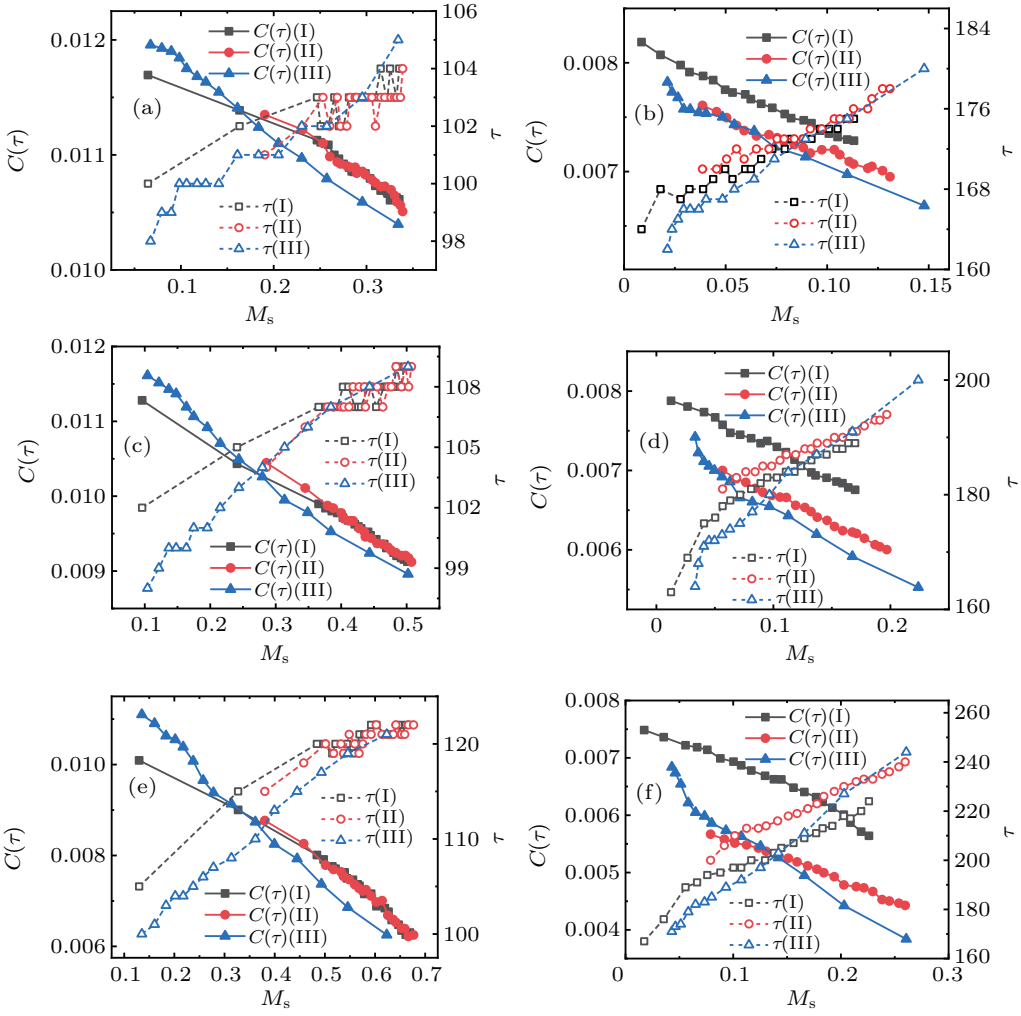


Fig. 9. Comparison of the results of the three strategies with M_s in the case of different μ and p_s: (a) $\mu = -2$, $p_s = 0.4$, (b) $\mu = 2$, $p_s = 0.4$, (c) $\mu = -2$, $p_s = 0.6$, (d) $\mu = 2$, $p_s = 0.6$, (e) $\mu = -2$, $p_s = 0.8$, (f) $\mu = 2$, $p_s = 0.8$. The value of M_s corresponds to different screening ranges in each case. The solid points represent $C(\tau)$ and hollow points represent τ. Each point is generated from 500 simulations of global infection.

Figures 9(a) and 9(b) show the comparison of the results respectively in the case of $\mu = -2$ and $\mu = 2$ under $p_s = 0.4$, and Figs. 9(c)–9(d) and Figs. 9(e)–9(f) show the comparison of the results in the case of different μ under $p_s = 0.6$ and $p_s = 0.8$. With the same value of M_s, the three strategies have similar effects on delaying epidemic spreading under $\mu = -2$, because most global moves and long-distance moves start or end in high-layer nodes. However, when μ gets larger, larger proportion of global moves and long-distance moves are between low-layer nodes. Thus, the differences in the effects between the strategies become larger. Besides, larger μ also weakens the role of high-layer nodes in accelerating spreading, thus strategy Ⅱ achieves smaller $C(\tau)$ and larger τ than strategy I with the same M_s.

Strategy Ⅲ has the worst effects when M_s is small. This is because for strategy Ⅲ, small M_s corresponds to large d_c, which means that moves of extremely long distance will be screened. In this case, moves between low-layer nodes account for a large proportion of the moves screened due to the long distance between them, which contribute less to the spreading velocity than moves into or out of high-layer nodes. As M_s increases, strategy Ⅲ can screen global moves, even moves between high-layer and low-layer nodes within a subnetwork. At the same time, strategy Ⅲ limits the moves of agents within the range of d_c, thus reduces the number of nodes whose agents can contact with each other. In contrast, strategy I does not reduce the move range of agents, and strategy Ⅱ only limits moves within each subnetwork. Therefore, when M_s increases, strategy Ⅲ reduces $C(\tau)$ and increases τ more obviously than strategies I and Ⅱ. When M_s is large enough, strategy Ⅲ has the best effects in reducing $C(\tau)$, while strategy I has the worst effects. However, strategy Ⅲ does not outperform other strategies in increasing τ, because it is less effective than strategies I and Ⅱ on screening moves into or out of high-layer nodes.

4. Conclusion and discussion

The objective of this paper is to probe into the mechanism of epidemic spreading in hierarchical geographical networks under different scenarios and deploy more targeted mitigation strategies to control epidemic spreading. We build an epidemic spreading model which consists of three sub-models: hierarchical geographical network model with periodic boundary conditions, human moving model with agents' preference for node layers and memory of initial nodes, and local infection model of SIR.

We investigate the spreading behavior of global infection under different scenarios, including different directions of human flow, different locations of infection source, and different moving behaviors of agents between each layer. We find that (1) epidemics in high layers always spread faster than in low layers regardless of the agents' preference for layers and location of infection source. Early infection in high layers and moving to high layers both accelerate the spreading process. (2) Travel of high-layer and low-layer residents have different effects on accelerating epidemic spreading. Travel of residents of high-layer nodes is more conducive to reducing the peak timing of new infected cases. Travel of residents of low-layer nodes is more conducive to increasing the peak value of new infected cases, but only when agents tend to move to high-layer nodes, and the effects of travel of low-layer residents on increasing the peak value is weakened when agents move to low-layer nodes. Moving between high and low layers increases the peak value of new infected cases more than moving in the same layer or between adjacent layers, and it also reduces the peak timing when the infection source is in the low layers. (3) Considering that low-layer residents pass more intermediate nodes in a move than high-layer residents, the infection in the intermediate nodes enhances the effects of the move of low-layer residents on epidemic spreading more than the effects of the move of high-layer residents. In general, moving to high-layer nodes and moving between subnetworks reduce the peaking timing of new infected cases, and moving between high and low layers increases the peaking value of new infected cases. Different from the previous studies that focus on nodes in high layers and with large degree, the findings highlight the role of agents in low-layer nodes in epidemic spreading, especially when infection in the intermediate nodes is considered.

Based on the above analysis, we have proposed screening strategies to reduce the risk of infectious disease spreading from two perspectives of node layer and moving distance and compared the inhibitory effects of different strategies. It is found that (1) screening moves into or out of high-layer nodes can screen out most global moves when agents move to high layers, but it is not effective when agents move to low layers. Screening long-distance moves achieves better effects when agents tend to move to low layers than to high layers. (2) With the same number of moves screened, improving the success rate is more effective than expanding the screening range for all three screening strategies. (3) With the same number of moves screened, the three strategies have similar results in delaying epidemic spreading when agents move to high layers. Screening moves into or out of high-layer nodes combined with screening moves between subnetworks has better results than only screening moves into or out of high-layer nodes when agents move to low layers. Screening long-distance moves has the worst results when the screening range is small, but it achieves better results as the screening range increases, and it has the best results in reducing the peak value of new infected cases when the screening range is large enough. In general, when we implement screening measures, increasing

the success rate of screening for high-layer nodes and long-distance moves should be a priority, followed by expanding the screening range. We should not only restrict agents from moving into or out of high-layer nodes, but also restrict agents from moving between subnetworks, and limiting the moving of agents to a relatively small range can effectively reduce the maximum number of new infected cases.

Our findings show that traffic network structure and human moving pattern both have important consequences on epidemic spreading. Preventing agents from moving to high-layer nodes, moving between subnetworks and between high and low layers is of great significance in delaying epidemic spreading. Control measures in the paper provide administrators with the best option under different scenarios.

References

[1] Kermack W O and McKendrick A G 1927 *Proc. Roy. Soc.* **115** 700
[2] Newman M E J 2002 *Phys. Rev. E* **66** 016128
[3] Keeling M J and Eames K T D 2005 *J. R. Soc. Interface* **2** 295
[4] Pastor-Satorras R and Vespignani A 2001 *Phys. Rev. E* **63** 066117
[5] Read J M and Keeling M J 2003 *Proc. R. Soc. B-Biol. Sci.* **270** 699
[6] Keeling M J and Rohani P 2002 *Ecol. Lett.* **5** 20
[7] Gallos L K and Argyrakis P 2004 *Phys. Rev. Lett.* **92** 138301
[8] Sattenspiel L and Dietz K 1995 *Math. Biosci.* **128** 71
[9] Yashima K and Sasaki A 2014 *PLoS One* **9** e98518
[10] Bajardi P, Poletto C, Ramasco J J, Tizzoni M, Colizza V and Vespignani A 2011 *PLoS One* **6** e16591
[11] Colizza V, Barrat A, Barthelemy M, Valleron A J and Vespignani A 2007 *PLoS Med.* **4** e13
[12] Eubank S, Guclu H, Kumar V S A, Marathe M V, Srinivasan A, Toroczkai Z and Wang N 2004 *Nature* **429** 180
[13] Colizza V, Barrat A, Barthelemy M and Vespignani A 2006 *Proc. Natl. Acad. Sci. USA* **103** 2015
[14] Colizza V, Pastor-Satorras R and Vespignani A 2007 *Nat. Phys.* **3** 276
[15] Hufnagel L, Brockmann D and Geisel T 2004 *Proc. Natl. Acad. Sci.* **101** 15124
[16] Lentz H H K, Selhorst T and Sokolov I M 2012 *Phys. Rev. E* **85** 066111
[17] Takaguchi T and Lambiotte R 2015 *J. Theor. Biol.* **380** 134
[18] Balcan D, Colizza V, Goncalves B, Hu H, Ramasco J J and Vespignani A *Proc. Natl. Acad. Sci. USA* **106** 21484
[19] Watts D J, Muhamad R, Medina D C and Dodds P S 2005 *Proc. Natl. Acad. Sci.* **102** 11157
[20] Han X P, Hao Q, Wang B H and Zhou T 2011 *Phys. Rev. E* **83** 036117
[21] Brockmann D, Hufnagel L and Geisel T 2006 ***439*** 462
[22] Zhao Z D, Liu Y and Tang M 2012 *Chaos* **22** 023150
[23] Han X P, Zhao Z D, Hadzibeganovic T and Wang B H 2014 *Commun. Nonlinear Sci. Numer. Simul.* **19** 1301
[24] Barabasi A L 2005 *Nature* **435** 207
[25] Paxson V and Floyd S 1994 *ACM SIGCOMM '94 Conference on Communication Architectures, Protocols and Applications* 31 August–2 September 1994 London, UK, p. 257
[26] Masoliver J, Montero M and Weiss G H 2003 *Phys. Rev. E* **67** 021112
[27] Iribarren J L and Moro E 2009 *Phys. Rev. Lett.* **103** 038702
[28] Min B, Goh K I and Vazquez A 2011 *Phys. Rev. E* **83** 036102
[29] Karsai M, Kivelä M, Pan R K, Kaski K, Kertész J, Barabasi A L and Saramäki J 2011 *Phys. Rev. E* **83** 025102
[30] González M C, Hidalgo C A and Barabási A L 2008 *Nature* **453** 779
[31] Ni S J and Weng W G 2009 *Phys. Rev. E* **79** 016111
[32] Wang P, González M C, Hidalgo C A and Barabási A L 2009 *Science* **324** 1071
[33] Granell C and Mucha P J 2018 *Phys. Rev. E* **97** 052302
[34] Balcan D and Vespignani A 2012 *J. Theor. Biol.* **293** 87
[35] Belik V, Geisel T and Brockmann D 2011 *Phys. Rev. X* **1** 011001
[36] Cao L, Li X, Wang B and Aihara K 2011 *Phys. Rev. E* **84** 041936
[37] Tang M, Liu L and Liu Z 2009 *Phys. Rev. E* **79** 016108
[38] Tang M, Liu Z and Li B 2009 *Europhys. Lett.* **87** 18005
[39] Ferguson N M, Cummings D A T, Fraser C, Cajka J C, Cooley P C and Burke D S 2006 *Nature* **442** 448
[40] Cowling B J, Lau L L H, Wu P, Wong H W C, Fang V J, Riley S and Nishiura H 2010 *BMC Infect. Dis.* **10** 82